


A novel design of circularly polarized ring CDRA with wideband impedance bandwidth using slotted microstrip feed line for X-band applications

Chandravilash Rai¹ , Sanjai Singh¹, Ashutosh Kumar Singh¹
and Ramesh Kumar Verma²

Research Paper

Cite this article: Rai C, Singh S, Singh AK, Verma RK (2022). A novel design of circularly polarized ring CDRA with wideband impedance bandwidth using slotted microstrip feed line for X-band applications. *International Journal of Microwave and Wireless Technologies* **14**, 1149–1158. <https://doi.org/10.1017/S1759078721001598>

Received: 23 August 2021
Revised: 1 November 2021
Accepted: 2 November 2021
First published online: 6 December 2021

Key words:

Circular polarization; inverted L-shaped; ring-CDRA; slotted microstrip feed line; tilted rectangular aperture

Author for correspondence:

Chandravilash Rai,
E-mail: cvrai87@gmail.com

¹Department of Electronics & Communication Engineering, Indian Institute of Information Technology Allahabad, Allahabad, U.P., India and ²Department of Electronics & Communication Engineering, Bundelkhand Institute of Engineering and Technology, Jhansi, U. P., India

Abstract

A circularly polarized ring cylindrical dielectric resonator antenna (ring-CDRA) of wideband impedance bandwidth is presented in this article. The proposed ring CDRA consist of an inverted rectangular (tilted rectangular) shaped aperture and inverted L-shaped slotted microstrip feed line. The tilted rectangular shaped aperture and inverted L-shaped microstrip feed line generate two-hybrid mode $HEM_{11\delta}$ and $HEM_{12\delta}$ while ring CDRA and slotted microstrip feed line are used for the enhancement of impedance bandwidth. The proposed ring CDRA is resonating between 6.08 and 12.2 GHz with 66.95% (6120 MHz) impedance bandwidth. The axial ratio (AR) bandwidth of 6.99% (780 MHz) is obtained between 10.76 and 11.54 GHz with a minimum AR value of 0.2 dB at a frequency of 11 GHz. The proposed geometry of ring CDRA has been validated with measurement performed by VNA and anechoic chamber. The operating range of the proposed radiator is useful for different applications in X-band.

Introduction

In the recent wireless communication era, a dielectric resonator (DR) is a more popular choice in the antenna field. Dielectric resonator antenna (DRA) has some benefits like high gain, large bandwidth, marginal cost, small size, higher radiation efficiency, various feeding method and low metallic losses to compare with planner antennas [1]. S. A. Long and his research team had demonstrated DRA and studied the field inside the DRA [2]. Since then, many researchers have worked and developed different types of DRA for various applications. DRA can be any shape such as cylindrical, rectangular, conical, hemispherical or any other shape but cylindrical and rectangular DRA are more popular due to design flexibility and easily available in the market [3].

In the last few years, researchers focus on enhancing the impedance bandwidth along with circular polarization (CP) characteristics of DRA. Various techniques are used for enhancement of bandwidth such as using simple slot feed DRA [4], stacked DRA of different permittivity using partial ground and excited with annular shape microstrip feed line [5], multilayered half split cylindrical dielectric resonator antenna (CDRA) using coaxial feed [6] provides impedance bandwidth of 63.7% (2850 MHz), CP stacked DRA using two pair of rectangular shape dielectric layer [7] excited via microstrip feed line provides AR bandwidth of 6% (600 MHz) and impedance bandwidth of 21% (600 MHz), stair-shape DRA using a pair of rectangular DR showing impedance bandwidth of 37% (2100 MHz) and 22% (1300 MHz) AR bandwidth [8], ring DRA using annular shape microstrip line feed with 66.72% (3710 MHz) impedance bandwidth at center frequency 5.35 GHz [9], hemispherical DRA having rectangular shape parasitic slot in the ground layer [10] and quarter CDRA [11] provides -10 dB bandwidth of 16.56% (390 MHz) and AR bandwidth of 3.6% (80 MHz). However, rectangular DRA of large size using tapered strip [12], cylindrical DRA excited by T-shape microstrip line [13] increases the -10 dB bandwidth from 12 to 26% and rectangular DRA using meandered-line and partial ground plane [14] showing impedance bandwidth of 20.67% along with 27.95% AR bandwidth are designed for the enhancement of bandwidth. Some other designs of DRA such as DR loaded circular shape microstrip patch [15], wideband DRA with CP characteristic using both rectangular as well as cubical DRA excited via conformal strip with L-shape line feed [16] showing 27.36% impedance bandwidth along with 23% AR bandwidth, bowtie-shape DRA excited with asymmetric cross-shape slot [17] offering 7.4% AR bandwidth with impedance bandwidth of 43.8%, cubical DRA excited with mark-shape microstrip line feed [18]

providing 35.35% impedance bandwidth and 20.62% AR bandwidth and hybrid DRA using four feed slots [19] for enhancing the bandwidth upto 50%. However, DRA with CP characteristic using semi-eccentric annular shape resonator [20] excited via probe feed shows -10 dB bandwidth of 29.14 and 5.71% AR bandwidth while CDRA excited with slot coupling [21] using microstrip feed line exhibits only 4% AR bandwidth and 16.77% impedance bandwidth. In the above reported DRA antennas, a lot of them are designed for bandwidth enhancement using different techniques but some of them have large size provided either narrow bandwidth or without CP characteristic. The essential condition for the generation of CP; two field components are equal in magnitude and orthogonal [15]. CP-DRA can be divided into two categories; single feed technique and double-feed technique. A single feed technique generates a narrow-band axial ratio (AR) [16] whereas double feed technique generates wideband AR [17] because of strong coupling between DRA and feed line [18] but the disadvantage of the double feed technique is that it has a bulky and complex structure [19].

In this paper, a circularly polarized ring CDRA is designed using an inverted rectangular (tilted rectangular) shaped aperture and inverted L-shaped slotted microstrip feed line. The inverted rectangular shaped aperture and inverted L-shaped slotted microstrip feed line excites two-hybrid $HEM_{11\delta}$ and $HEM_{12\delta}$ mode. The impedance bandwidth and AR bandwidth both have been improved by step by step designing and a lot of parametric variations like (i) with and without DRA (ii) with and without slotted line feed (iii) radius of ring CDRA (iv) length of the slot, and (v) position of rectangular (tilted) shaped aperture. E-field distribution of inside the ring CDRA and radiation pattern is also described by some mathematical equations. Besides these observations, the geometry of the proposed ring CDRA has been validated with measurement performed by VNA and anechoic chamber. The proposed radiator is resonating between 6.08 and 12.2 GHz with 66.95% (6120 MHz) impedance bandwidth. The AR bandwidth is obtained 6.99% (780 MHz) between 10.76 and 11.54 GHz. Moreover, the frequency band of range 6.41–7.38 GHz comes under the category of extended C-band application and is useful for earth-space communication [22] while the frequency band 10.2–12.2 GHz is widely employable for the reception of fixed service satellite (FSS) and direct broadcast satellite (DBS) services [23].

The upcoming content of the proposed work is organized in the following sections. The geometry and parameters of the proposed ring CDRA are shown in section “Geometry of proposed ring CDRA” while the working operation of the proposed ring CDRA along with step by step design and generation of circular wave are discussed in the section “Working of proposed ring CDRA”. In section “Results discussion and experimental validation”, results discussion along with experimental validation and performances comparison of proposed ring CDRA with previous work are discussed. Finally, the conclusion of the proposed ring CDRA is described in section “Conclusion”.

Geometry of proposed ring CDRA

The geometry of the proposed ring CDRA of overall size $L \times W$ mm² is shown in Fig. 1. Inverted rectangular (tilted rectangular) shaped aperture ($a \times b$ mm²) has been etched on the top of the substrate (FR-4: $\epsilon_{rsub} = 4.4$, $\tan \delta = 0.02$ and height = 1.6 mm) and an inverted L-shaped slotted (slot length $e = 5.25$ mm and

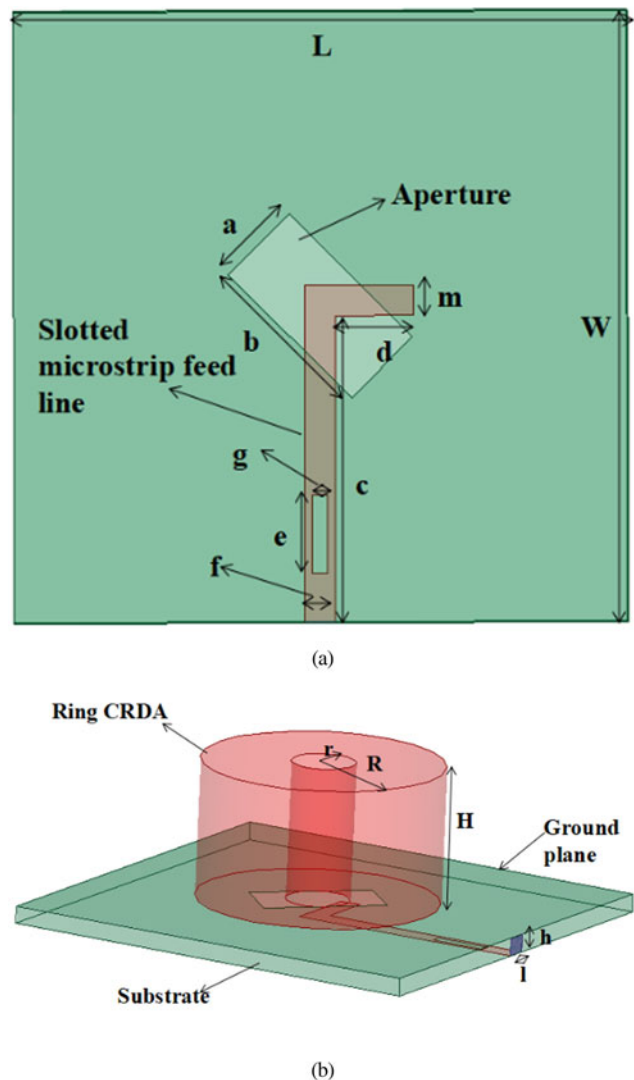


Fig. 1. (a) Systematic diagram of proposed ring CDRA. (b) Feeding structure in isometric view.

width $g = 1$ mm) microstrip feed line (feed length $c = 20$ mm and width $f = 2$ mm) is designed below the substrate as shown in Fig. 1(a). The ring CDRA (Alumina: $\epsilon_r = 9.8$, $\tan \delta = 0.002$) of height of 12.75 mm having inner radius of 3 mm and outer radius of 11 mm is positioned on the substrate with the help of adhesive material as shown in Fig. 1(b). The fabricated prototype of the proposed ring CDRA is shown in Fig. 2. The details of optimized parameters are shown in Table 1.

Working of proposed ring CDRA

Ansys HFSS simulator is used to analyze the working of the proposed ring CDRA. The proposed ring CDRA is simulated between frequency ranges 6–13 GHz. The working of the proposed ring CDRA is divided into two sub-sections: (i) Return loss $|S_{11}|$ and (ii) CP wave analysis. Besides stepwise design, the return loss $|S_{11}|$ analysis was carried out to observe the effect on impedance bandwidth in terms of ring CDRA (without DRA, with CDRA, with ring CDRA and variation in radius of ring CDRA), microstrip feed line (without slotted, with slotted and slot length variation) and position of rectangular-shaped

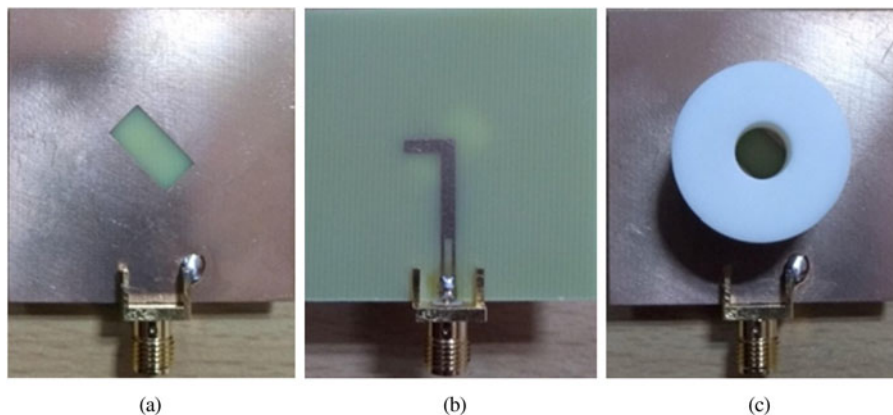


Fig. 2. Fabricated prototype of proposed ring CDRA. (a) Top view without ring CDRA. (b) Feeding structure. (c) Top view with ring CDRA.

aperture (angle variation of tilted rectangular aperture) whereas CP wave analysis carried out to observed the effect on AR bandwidth in terms of microstrip feed line (slot length variation) and position of rectangular-shaped aperture (angle variation of tilted rectangular aperture).

Return loss $|S_{11}|$ analysis

A stepwise design procedure of the proposed ring CDRA is shown in Fig. 3 and the commensurate $|S_{11}|$ graph for each step are shown in Fig. 4. It is clear from Fig. 4, that in step-1, ring CDRA is resonating as a multiband antenna due to two rhombus-shaped apertures and a simple rectangular microstrip feed line. In step-2, ring CDRA is resonating as a dual-band antenna due to an inverted rectangular (tilted rectangular) shaped aperture and simple rectangular microstrip feed line. In step-3 and step-4, the antenna is resonated nearly the same frequency range, but bandwidth enhancement in step-4 is due to the slotted microstrip feed line.

Effect of ring CDRA

The $|S_{11}|$ graph of without DRA, with CDRA and with ring CDRA is shown in Fig. 5. It is confirmed from Fig. 5 that the proposed ring CDRA is a hybrid radiator because the resonating band is due to with and without DRA. The ring CDRA has better bandwidth than CDRA (without ring) due to removing the central portion of ceramic material. (Decreasing the Q-factor and increasing the impedance bandwidth) [24]. The antenna is resonating in dual-band with and without DRA while in wideband with ring CDRA.

The $|S_{11}|$ graph variation after changing the radius (r) of ring CDRA is shown in Fig. 6. It is confirmed from Fig. 6 that the $|S_{11}|$ graph of the proposed ring CDRA at radius $r = 3$ mm is better in terms of impedance bandwidth. Besides radius $r = 3$ mm, the antenna is resonating in a dual band at radius $r = 2$ mm, $r = 2.5$ mm and $r = 3.5$ mm while resonating in a triple band at radius $r = 4$ mm.

Effect of the slotted feed line

Figure 7 represents the $|S_{11}|$ graph with slotted microstrip feed line (slot length $e = 5.25$ mm and width $g = 1$ mm) and without slotted microstrip feed. It is clear from Fig. 7, that the proposed ring CDRA with slotted microstrip feed line is resonating below -10 dB line between 6.08 and 12.2 GHz frequency band, but in case of without slotted microstrip feed line, some part in the

Table 1. Optimized parameters of the proposed ring CDRA.

Symbols	Dimension (mm)	Symbols	Dimension (mm)
a	5.65	H	12.75
b	11.31	h	1.6
c	20	l	2
d	5.1	R	11
e	5.25	r	3
f	2	m	2
g	1	L, W	40

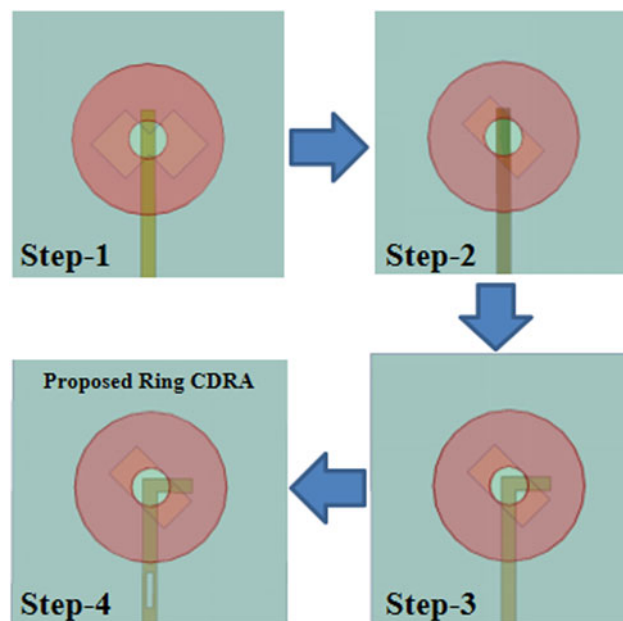


Fig. 3. Stepwise design of proposed ring CDRA.

given frequency band (6.08–12.2 GHz) is resonating above the -10 dB line. Thus, the proposed ring CDRA with slotted microstrip feed line has better impedance bandwidth because of providing good coupling between antenna and feed line [25, 26].

The variation of $|S_{11}|$ graph after changing the slot length (e) is shown in Fig. 8. The variation in slot length is observed at

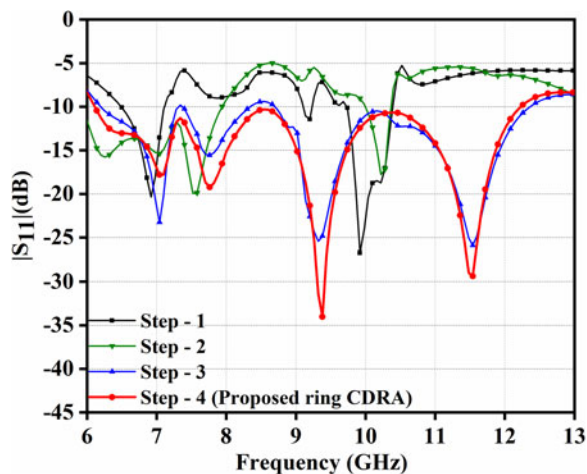


Fig. 4. Change in $|S_{11}|$ graph with step to step design procedure.

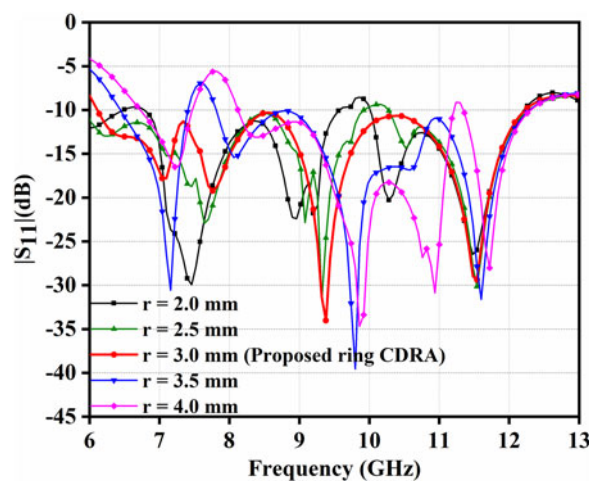


Fig. 6. Comparison of $|S_{11}|$ graph after changing the radius of ring CDRA.

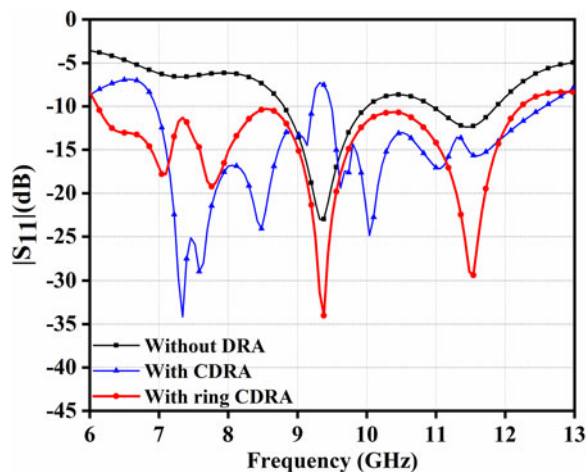


Fig. 5. Comparison of $|S_{11}|$ graph without DRA, with CDRA and with ring CDRA.

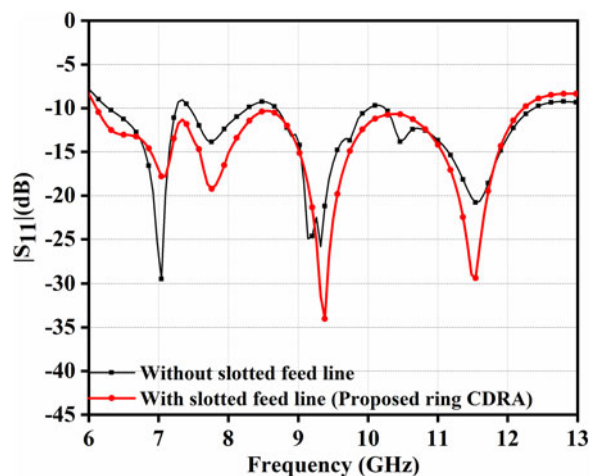


Fig. 7. Comparison of $|S_{11}|$ graph with and without slotted microstrip line feed.

different values of slot length between $e = 4.25$ mm to $e = 5.75$ mm. It is clear from Fig. 8, that the proposed ring CDRA is optimal at $e = 5.25$ mm with a small improvement in impedance bandwidth while a large effect is observed in AR bandwidth.

Effect of the tilted rectangular (inverted rectangular shaped) aperture

Figure 9 represents the changing position of a rectangular-shaped aperture with an angle (θ) and its commensurate $|S_{11}|$ graph is depicted in Fig. 10. It is confirmed from Fig. 10 that the proposed ring CDRA at $\theta = 45^\circ$ is resonating below -10 dB line with wide-band impedance bandwidth in the frequency band 6.08–12.2 GHz while the antenna is resonating in multiband for other angles except $\theta = 45^\circ$. Thus, the impedance bandwidth of the proposed ring CDRA at $\theta = 45^\circ$ is better than other angles.

E-field distribution inside the ring CDRA at frequencies 6.4 and 11.5 GHz is shown in Fig. 11. It is confirmed from Fig. 11 (a) that $HEM_{11\delta}$ mode is generated at frequency 6.4 GHz whereas Fig. 11(b) shows the generation of a higher $HEM_{12\delta}$ mode at frequency 11.5 GHz [27]. The $HEM_{11\delta}$ mode is a fundamental mode in ring CDRA which shows one full wave variation in the azimuthal direction and one half-wave variation in a radial direction.

Similarly, $HEM_{12\delta}$ mode shows one full wave variation in the azimuthal direction and two half-wave variation in a radial direction. In both modes, “ δ ” shows the variation in an axial direction and its values lies between 0 and 1 [1, 28]. In the dielectric waveguide, the boundary condition is not perfect compared to the metallic waveguide, so the field line cannot rotate completely and the direction of propagation is neither completely zero nor one [16].

The generated modes can also verify by using the following mathematical formulas [28, 29].

$$f_r \text{ HEM}_{11\delta} = \frac{6.324c}{2\pi r \sqrt{\epsilon_{dra}} + 2} \left\{ 0.27 + 036 \frac{r}{2H} + 0.02 \left(\frac{r}{2H} \right)^2 \right\} \quad (1)$$

We can calculate the $f_r \text{ HEM}_{12\delta}$ with the help of $f_r \text{ HEM}_{11\delta}$:

$$f_r \text{ HEM}_{12\delta} \geq 1.8 \times f_r \text{ HEM}_{11\delta} \quad (2)$$

where, r = internal radius of ring dielectric resonator and H =

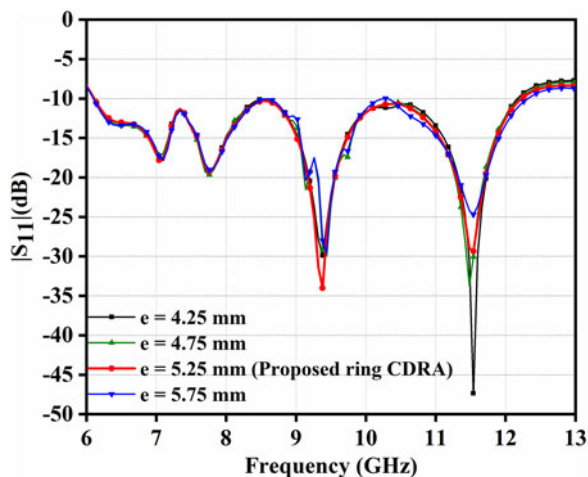


Fig. 8. Comparison of $|S_{11}|$ graph after changing the length of the slot.

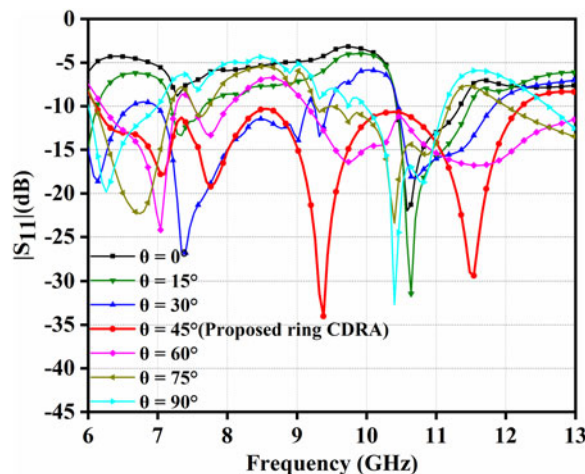


Fig. 10. The variation of $|S_{11}|$ graph at different position of rectangular-shaped aperture.

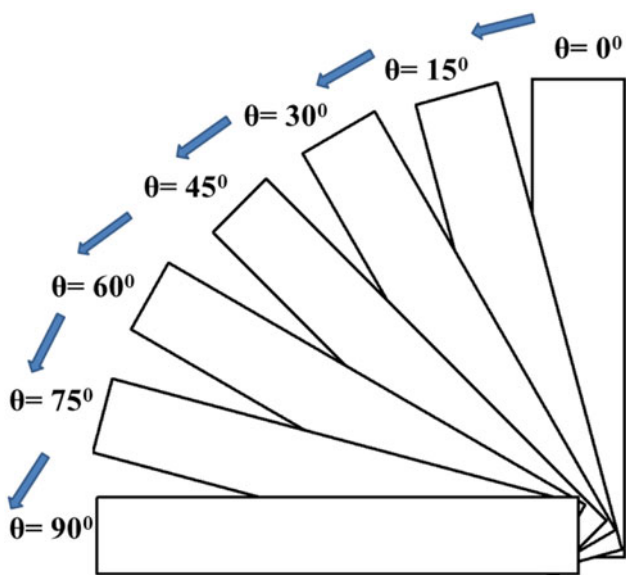


Fig. 9. Position of rectangular (tilted) shaped aperture at a different angle (θ).

height of ring dielectric resonator.

$$\epsilon_{dra} = \left[\frac{9.8(V_{Alumina}) + V_{Ring}}{V_{Alumina} + V_{Ring}} \right] \tag{3}$$

where,

$$V_{Alumina} = V_{Cylindrical} - V_{Ring} \tag{4}$$

From equations (1) and (2), the resonating frequency of mode $HEM_{11\delta}$ is found 6.4 GHz while for mode $HEM_{12\delta}$ it is found 11.5 GHz.

Circular wave (CP) analysis

Figure 3 represents the step by step design procedure and its corresponding AR versus frequency graph is shown in Fig. 12. The essential condition for the creation of CP wave; two field

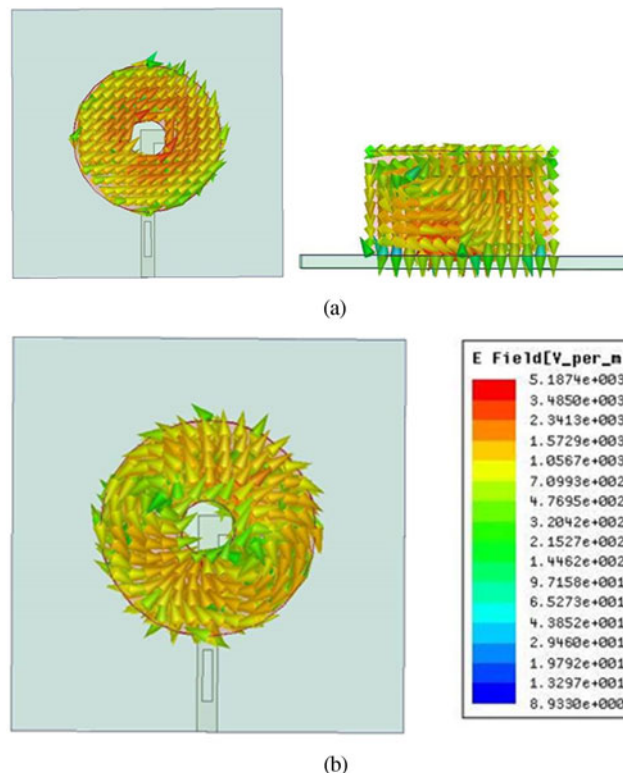


Fig. 11. The distribution of E-field in ring CDRA. (a) Top view and side view at 6.4 GHz. (b) Top view at 11.5 GHz.

components are equal in magnitude and orthogonal to each other [14]. It is clearly observed from Fig. 12, that the CP wave is not generated in step-1 and step-2. The tilted rectangular shaped aperture and inverted L-shaped microstrip feed line are responsible for generating CP waves in steps-3 and step-4 with AR bandwidth of 2.13% (230 MHz) and 6.99% (780 MHz) respectively. In the proposed ring CDRA, tilted rectangular shaped slot behaves as a magnetic dipole and is also used to maintain the equal amplitude of the fields [30]. The inverted L-shaped feed line acts as an electric dipole and provides the phase

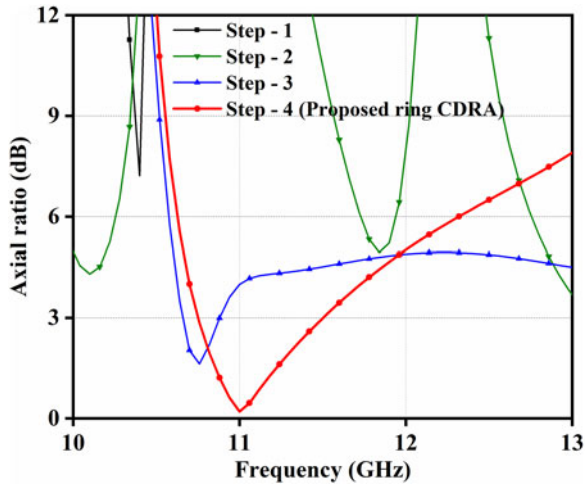


Fig. 12. Generation of circular wave with step to step design procedure.

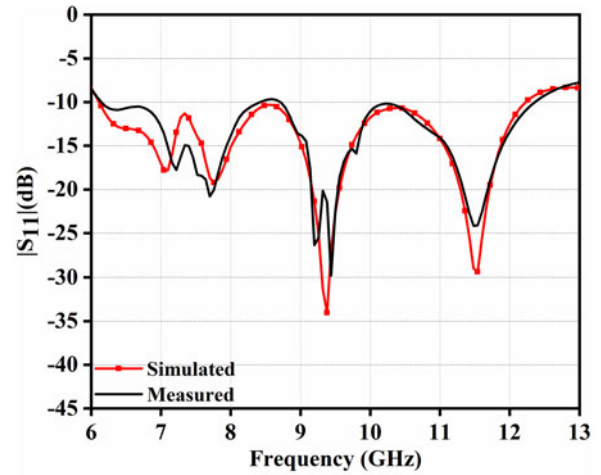


Fig. 15. Comparison measured and simulated of $|S_{11}|$ graph.

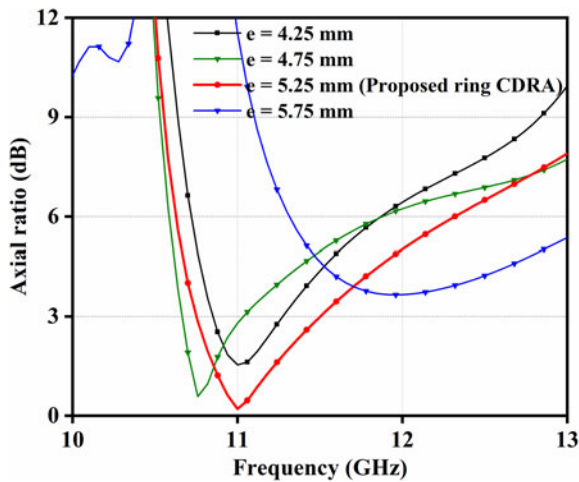


Fig. 13. Comparison of AR graph after altering slot length.

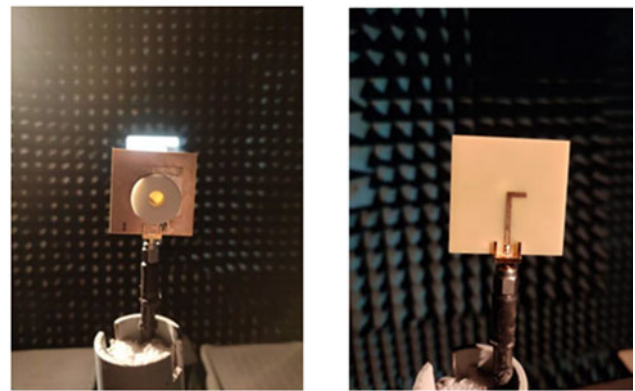


Fig. 16. Image of measurement set up in an anechoic chamber.

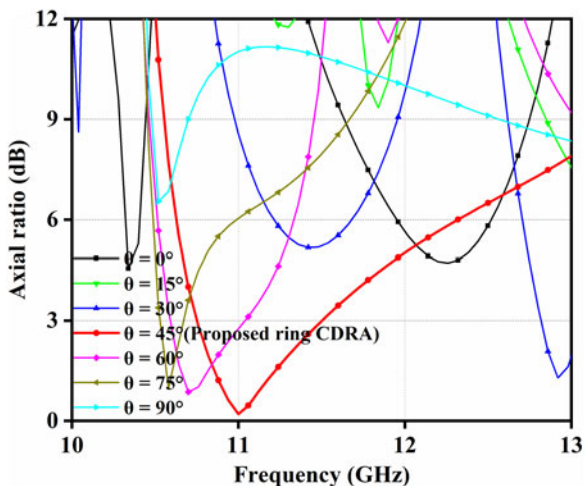


Fig. 14. The variation of AR graph after changing the position of rectangular-shaped aperture with angle (θ).

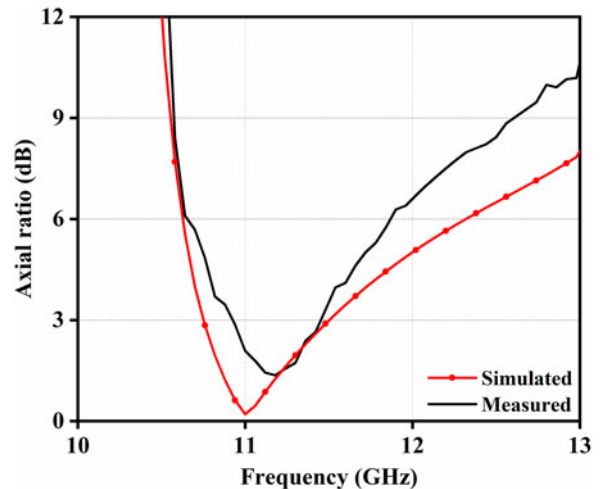


Fig. 17. Comparison of measured and simulated AR graph.

difference (90°) between the fields [29]. Thus, the tilted rectangular shaped aperture and inverted L-shaped microstrip feed line are used to generate CP wave. However, the enhancement of AR bandwidth in step-4 is due to the slotted microstrip feed line (strong coupling between antenna and feed line) [25, 26].

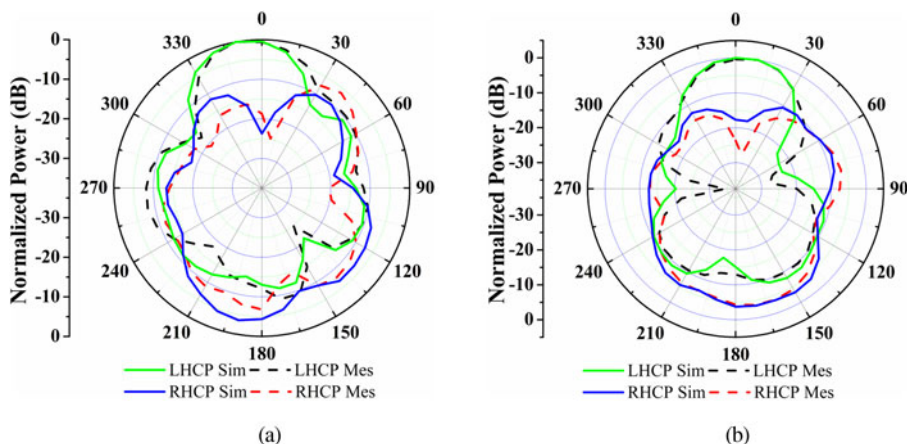


Fig. 18. LHCP/RHCP pattern of proposed ring CDRA at 11 GHz for (a) $\theta=0, \phi=0$, (b) $\theta=0, \phi=90$.

The variation of AR bandwidth with changing the slot length of the microstrip feed line between $e = 4.25$ mm to $e = 5.75$ mm is shown in Fig. 13. It is confirmed from Fig. 13, that the optimized value of slot length is observed at $e = 5.25$ mm for maximum AR bandwidth 6.99% (780 MHz) compared to $e = 4.25$ mm (450 MHz) and $e = 4.75$ mm (390 MHz) while no AR bandwidth is obtained for $e = 5.75$ mm.

The position of tilted rectangular shaped aperture is changed at a different angle (θ) between $\theta = 0^\circ$ and $\theta = 90^\circ$ as shown in Fig. 9 and its corresponding AR versus frequency graph is depicted in Fig. 14. It is confirmed from Fig. 14 that the AR graph only for angles $\theta = 45^\circ, \theta = 60^\circ$ and $\theta = 75^\circ$ are resonating below 3 dB AR line, but the 3 dB AR bandwidth 6.99% (780 MHz) of the proposed ring CDRA at angle $\theta = 45^\circ$ is better than angle $\theta = 60^\circ$ (450 MHz) and $\theta = 75^\circ$ (160 MHz). The rectangular (tilted) shaped aperture is used for maintaining the equal amplitude of two fields [30].

Results discussion and experimental validation

The experimental outcomes are compared with the simulated results for verifying the design of the proposed radiator with help of a prototype antenna as shown in Fig. 2. Vector network analyzer (Agilent Technologies E5071C) is used to measure the proposed radiator’s return loss $|S_{11}|$ graph. A comparison of measured and simulated $|S_{11}|$ graph is shown in Fig. 15. The return loss $|S_{11}|$ graphs are almost the same. Some changes in the return loss $|S_{11}|$ graph take place because of the use of gluey materials for the placing of ring CDRA above the substrate [31]. The experimental return loss $|S_{11}|$ graph shows that the proposed radiator is resonating between 6.14 and 12.32 GHz with 66.95% (6180 MHz) impedance bandwidth whereas simulated antenna also shows 66.95% impedance bandwidth but resonating between 6.08 and 12.2 GHz (6120 MHz).

The anechoic chamber as shown in Fig. 16 is used to measure the far-field pattern of the proposed ring CDRA, where the CP horn antenna is used as a reference antenna. The comparison of AR graphs between measured and simulated is shown in Fig. 17. The dual pattern measurement method is used to measure the AR [32]. A good similarity is achieved between measured and simulated AR graphs. The simulated 3 dB AR bandwidth is obtained 6.99% (780 MHz) between the frequency ranges of 10.76–11.54 GHz whereas the experimental result shows that the proposed radiator is resonating between 10.9 and 11.5 GHz with a 5.36% (600 MHz) AR bandwidth. The minimum AR value of 0.2 and 1.36 dB is obtained for the simulated and measured antenna at 11 and 11.2 GHz respectively.

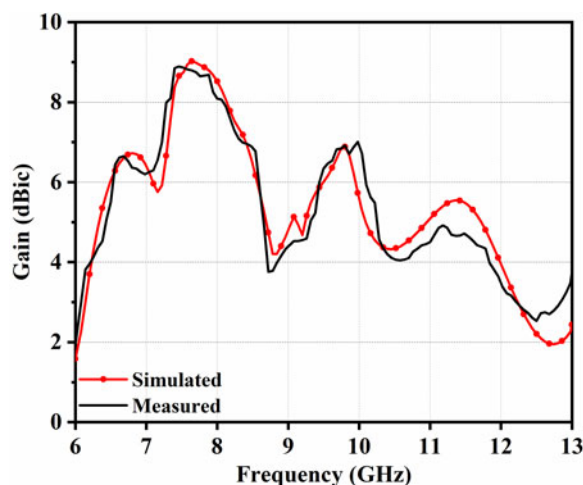


Fig. 19. Comparison of measured and simulated gain.

Measured and simulated LHCP (left hand circularly polarized) and RHCP (right hand circularly polarized) pattern in broadside direction at $\theta = 0, \phi = 0$ and $\theta = 0, \phi = 90$ are shown in Figs 18(a) and 18(b) respectively at frequency 11 GHz. It is clear from Fig. 18 that the proposed ring CDRA exhibits an LHCP pattern with 20 dB difference between LHCP and RHCP patterns and a good similarity between measured and simulated results is observed. The radiation pattern can be improved by reducing the thickness of the substrate [33], but after decreasing the thickness of the substrate, bandwidth also decreases [34]. The radiation pattern of the horizontal (E_H) and vertical plane (E_V) is used to measure the LHCP and RHCP pattern of the proposed ring CDRA [35].

$$E_{LHCP} = \frac{1}{\sqrt{2}}(E_H - jE_V) \tag{5}$$

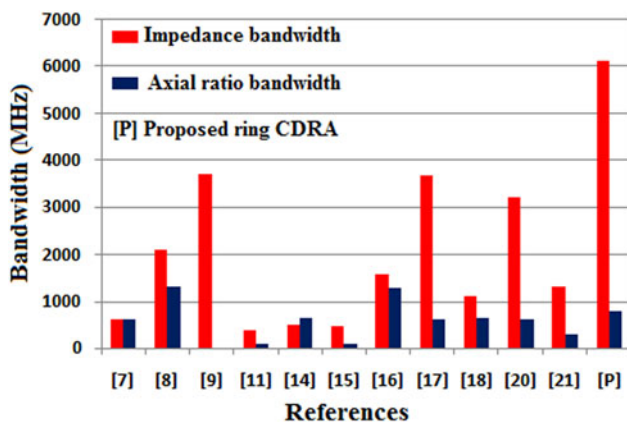
$$E_{RHCP} = \frac{1}{\sqrt{2}}(E_H + jE_V) \tag{6}$$

The measured and simulated gain in the broadside direction (at $\theta = 0, \phi = 0$) is shown in Fig. 19. A good similarity is seen between a measured and simulated gain of the proposed ring

Table 2. Comparison of proposed ring CDRA with previous published wideband DRA.

Type of DRA	Size of antenna (mm)	No. of DRA	Feeding method	Impedance bandwidth (%)	AR bandwidth (%)	Peak gain (dB)
Stacked DRA [7]	40 × 40 × 0.8	4	Microstrip feed line	21 (600 MHz)	6 (600 MHz)	6.7
Stair shaped DRA [8]	50 × 50 × 0.8	2	A trapezoidal patch is used as a feed mechanism	37 (2100 MHz)	22 (1300 MHz)	5.7
Ring CDRA [9]	50 × 48 × 1.6	1	Microstrip feed line	66.72 (3710 MHz)	NR	4.31
Quarter CDRA [11]	150 × 150 × 3.5	1	Probe feed	16.56 (390 MHz)	3.6 (80 MHz)	6.72
RDRA [14]	40 × 40 × 1.6	2	Meandered-line inductor feed	20.67 (500 MHz)	27.95 (650 MHz)	2.3
DR loaded patch [15]	100 × 100 × 4.8	1	Probe feed	19.2 (460 MHz)	3.7 (90 MHz)	8.6
RDRA [16]	40 × 40 × 1.6	2	Conformal-strip and inverted L-shaped microstrip-feed-line	27.36 (1580 MHz)	23 (1290 MHz)	5.92
Bowtie-shape DRA [17]	61 × 61 × 0.8	1	Asymmetric cross-shape slot using microstrip feed	43.8 (3680 MHz)	7.8 (600 MHz)	5.8
Cubical DRA [18]	40 × 40 × 1.6	1	Microstrip feed	35.35 (1100 MHz)	20.62 (650 MHz)	1.51
Semi-eccentric annular DR [20]	35 × 35 × 4.5	1	Probe feed	29.14 (3210 MHz)	5.71 (610 MHz)	4.78
CDRA [21]	40 × 40 × 1.6	1	Microstrip line	16.77 (1300 MHz)	4 (300 MHz)	5.92
Proposed Ring CDRA	40 × 40 × 1.6	1	Microstrip feed line	66.95 (6120 MHz)	6.99 (780 MHz)	9.02

NR: not reported.

**Fig. 20.** Bandwidth comparison of proposed ring CDRA with reported work.

CDRA. It is observed from Fig. 19 that the highest gain value of 9.02 dBic is obtained at 7.6 GHz while the peak gain value of 5.7 and 5.4 dBic is obtained at resonating peaks 9.4 and 11.5 GHz respectively. However, 5.08 dBic peak gain is obtained at 11 GHz in the AR band. It is clear from Fig. 5 that the lower part of the frequency band is due to CDRA but the upper half portion is due to the combining effect of inverted rectangular shaped (tilted) aperture and ring CDRA. Thus, the gain is not constant and decreasing at the upper portion of the frequency band due to metallic loss [35].

Table 2 represents the comparison of the proposed ring CDRA with previous published wideband DRA based on the size of the antenna, no. of DRA used, feeding method, impedance bandwidth, AR bandwidth and peak gain whereas bar graph shown in Fig. 20 represents a comparison of impedance and AR bandwidth. It is confirmed from Table 2 and Fig. 20 that the proposed ring CDRA has numerous advantages such as simple in design (small structure and single DRA is used), large impedance

bandwidth (6120 MHz) and high peak gain (9.02 dB) as compared to reported papers but the AR (780 MHz) is less only compared to single-band antennas [8] (1300 MHz) and [16] (1290 MHz). However, their impedance BW is narrow (2100 and 1580 MHz) compared to the proposed ring CDRA and they also used two DRA. The size of antennas represented in [8, 9, 11, 15, 17] is also large compared to proposed ring CDRA whereas proposed ring CDRA is superior in terms of peak gain compared to previous published wideband DRA shown in Table 2.

Conclusion

In this article, a circularly polarized ring CDRA of wideband impedance bandwidth has been presented. The proposed ring CDRA provides two hybrid modes HEM_{118} and HEM_{128} resonating between frequency band 6.08–12.2 GHz with 66.95% (6120 MHz) impedance bandwidth. The AR bandwidth is obtained at 6.99% (780 MHz) with a minimum AR value of 0.2 dB at frequency 11 GHz between the frequency ranges of 10.76–11.54 GHz. The use of inverted rectangular (tilted rectangular) shaped aperture and inverted L-shaped microstrip feed line generates two-hybrid mode HEM_{118} and HEM_{128} while ring CDRA and slotted microstrip feed line are responsible for the enhancement of impedance bandwidth. The proposed ring CDRA shows a peak gain of 9.02 dBic at 7.6 GHz whereas 5.08 dBic peak gain is obtained at 11 GHz in the AR band. The resonating band of a proposed radiator is useful for different applications in X-band.

Data availability statement

Data sharing not applicable – no new data generated.

Conflict of interest. The author declares no potential conflict of interest.

References

1. **Petosa A** (2007) *Dielectric Resonator Antenna Handbook*. Norwood, MA: Artech House.
2. **Long SA, McAllister MW and Shen LC** (1983) The resonant dielectric cavity antenna. *IEEE Transactions on Antennas and Propagation* **31**, 406–412.
3. **Luk KM and Leung KW** (2003) *Dielectric Resonator Antennas*. Philadelphia: Baldock, Hertfordshire, England.
4. **Ittipiboon A, Petosa A, Roscoe D and Cuhaci M** (1996) An investigation of a novel broadband dielectric resonator antenna. *IEEE Antennas and Propagation Society International Symposium* **3**, 2038–2041.
5. **Sharma A and Gangwar RK** (2016) Asymmetrical annular shape microstrip line fed stacked cylindrical dielectric resonator antenna for UWB. *2016 Asia-Pacific Microwave Conference (APMC)*, pp. 1–4.
6. **Chaudhary RK, Srivastava KV and Biswas A** (2012) Wideband multi-layer multi-permittivity half-split cylindrical dielectric resonator antenna. *Microwave and Optical Technology Letters* **54**, 2587–2590.
7. **Fakhte S, Oraizi H and Karimian R** (2014) A novel low-cost circularly polarized rotated stacked dielectric resonator antenna. *IEEE Antennas and Wireless Propagation Letters* **13**, 722–725.
8. **Fakhte S, Oraizi H, Karimian R and Fakhte R** (2015) A new wideband circularly polarized stair-shaped dielectric resonator antenna. *IEEE Transactions on Antennas and Propagation* **63**, 1828–1832.
9. **Chaudhary RK, Kumar R and Srivastava KV** (2013) Wideband ring dielectric resonator antenna with annular-shaped microstrip feed. *IEEE Antennas and Wireless Propagation Letters* **12**, 595–598.
10. **So KK and Leung KW** (2005) Bandwidth enhancement and frequency tuning of the dielectric resonator antenna using a parasitic slot in the ground plane. *IEEE Transactions on Antennas and Propagation* **53**, 4169–4172.
11. **Bezerra JWO, Sousa DG, Junqueira CCM, Silva MAS, Barroso GC and Sombra ASB** (2015) Circularly polarized quarter-cylinder-shaped dielectric resonator antenna using a single probe feed. *Microwave and Optical Technology Letters* **57**, 722–726.
12. **Khalily M, Rahim MKA and Kishk AA** (2011) Bandwidth enhancement and radiation characteristics improvement of rectangular dielectric resonator antenna. *IEEE Antennas and Wireless Propagation Letters* **10**, 393–395.
13. **Bijumon PV, Menon SK, Suma MN, Sebastian MT and Mohanan P** (2005) Broadband cylindrical dielectric resonator antenna excited by modified microstrip line. *Electronics Letters* **41**, 385–387.
14. **Kumar R and Chaudhary RK** (2017) Wideband circularly polarized dielectric resonator antenna coupled with meandered-line inductor for ISM/WLAN applications. *International Journal of RF and Microwave Computer-Aided Engineering* **27**, 1–7.
15. **Tsai CL, Deng SM, Chen TW and Liu LW** (2009) Circularly polarized dielectric resonator loaded circular microstrip patch antennas for WLAN 2.4 GHz applications. *Microwave and Optical Technology Letters* **51**, 1470–1473.
16. **Kumar R and Chaudhary RK** (2016) A wideband circularly polarized dielectric resonator antenna excited with conformal-strip and inverted L-shaped microstrip-feed-line for WLAN/WI-MAX applications. *Microwave and Optical Technology Letters* **58**, 2525–2531.
17. **Chauthaiwale P, Chaudhary RK and Srivastava KV** (2015) Circularly polarized bowtie-shaped dielectric resonator antenna excited with asymmetric cross slot. *Microwave and Optical Technology Letters* **57**, 1723–1727.
18. **Kumar R and Chaudhary RK** (2016) A wideband circularly polarized cubic dielectric resonator antenna excited with modified microstrip feed. *IEEE Antennas and Wireless Propagation Letters* **15**, 1285–1288.
19. **Massie G, Caillet M, Clenet M and Antar YMM** (2010) A new wideband circularly polarized hybrid dielectric resonator antenna. *IEEE Antennas and Wireless Propagation Letters* **9**, 347–350.
20. **Lee JM, Kim SJ, Kwon G, Song CM, Yang Y, Lee KY and Hwan KC** (2015) Circularly polarized semi-centric annular dielectric resonator antenna for X-band applications. *IEEE Antennas and Wireless Propagation Letters* **14**, 1810–1813.
21. **Dash SKK, Khan T and Kanaujia BK** (2017) Wideband circularly polarized cylindrical dielectric resonator antenna for X-band applications. *Microwave and Optical Technology Letters* **59**, 2463–2468.
22. **Chahat N, Decrossas E, Ovejero DG, Yurduseven O, Radway MJ, Hodges RE, Estabrook P, Baker JD, Bell DJ, Cwik TA and Chattopadhyay G** (2019) Advanced CubeSat antennas for deep space and earth science missions: a review. *IEEE Antennas and Propagation Magazine* **61**, 37–46.
23. **Kumar R, Saini GS and Singh D** (2020) Compact tri-band patch antenna for KU band applications. *Progress In Electromagnetics Research C* **103**, 45–58.
24. **Sharma A, Ranjan and P and Sikandar** (2021) Dual-band ring-shaped dielectric resonator-based radiator with left and right-handed sense circularly polarized features. *IETE Technical Review* **38**, 511–519.
25. **Zebiri C, Benabelaziz F, Lashab M, Sayad D, Elmecri F, Elfegani ITE, Ali NT, Hussaini AS, Abd-Alhameed RA and Rodriguez J** (2016) Aperture-coupled asymmetric dielectric resonator antenna with slotted microstrip line for enhanced ultrawideband. *2016 10th European Conference on Antennas and Propagation (EuCAP)*, 1–3.
26. **Shivnarayan and Vishvakarma BR** (2004) Analysis of slot loaded microstrip patch antenna. *IEEE Antennas and Propagation Society International Symposium* **3**, 2420–2423.
27. **Kajfez D, Glisson AW and James J** (1984) Computed modal field distributions for isolated dielectric resonators. *Microwave Theory and Techniques, IEEE Transactions on* **32**, 1609–1616.
28. **Mongia RK and Bhartia P** (1994) Dielectric resonator antennas—a review and general design relations for resonant frequency and bandwidth. *International Journal of Microwave and Millimeter-Wave Computer-Aided Engineering* **4**, 230–247.
29. **Sharma A, Das G and Gangwar RK** (2017) Dual-band dual-polarized hybrid aperture-cylindrical dielectric resonator antenna for wireless applications. *International Journal of RF and Microwave Computer-Aided Engineering* **27**, 1–9.
30. **Almpanis G, Fumeaux C and Vahldieck R** (2006) Offset cross-slot-coupled dielectric resonator antenna for circular polarization. *IEEE Microwave and Wireless Components Letters* **16**, 461–463.
31. **Sharma A, Das G and Gangwar RK** (2018) Design and analysis of tri-band dual-port dielectric resonator-based hybrid antenna for WLAN/WiMAX applications. *IET Microwaves, Antennas and Propagation* **12**, 986–992.
32. **Stutzman WL and Garg GA** (2013) *Antenna Theory and Design*. Hoboken, NJ: A JohnWiley& Sons.
33. **Nguyen TK, Tran H and Nguyen-Trong N** (2017) A wideband dual-cavity-backed circularly polarized crossed dipole antenna. *IEEE Antennas and Wireless Propagation Letters* **16**, 3135–3138.
34. **Schaubert DH, Pozar DM and Adrian A** (1989) Effect of microstrip antenna substrate thickness and permittivity: comparison of theories with experiment. *IEEE Transactions on Antennas and Propagation* **37**, 677–682.
35. **Sharma A, Das G and Gangwar RK** (2017) Dual-band circularly polarized hybrid antenna for WLAN/WiMAX applications. *Microwave and Optical Technology Letters* **59**, 2450–2457.



Chandrivilash Rai is currently working as a research scholar in the Department of Electronics & Communication Engineering, Indian Institute of Information Technology Allahabad, Prayagraj, U.P (India). In 2009, he received his B. Tech Degree in electronics and communication engineering from the UPTU, Lucknow, and completed M.Tech in digital communication engineering from Rajiv Gandhi Proudyogiki Vishwavidyalaya, University in Bhopal, Madhya Pradesh, India, in 2017. His research interests include RF and microwave, dielectric resonator antenna, microstrip patch antennas, wireless communication and antenna theory.



Dr. Sanjai Singh received his Ph.D. degree from the University of Allahabad, India. Currently, he is an associate professor at the Electronics and Communication Engineering Department at the Indian Institute of Information Technology, Allahabad, India. His research interests are modern physics, semiconductor devices, wave theory, antenna theory.



Dr. Ashutosh Kumar Singh received his M. Tech. degree from MNNIT Allahabad and a Doctoral degree from the Indian Institute of Information Technology, Allahabad, India. Currently, he is an assistant professor at the Electronics and Communication Engineering Department at the Indian Institute of Information Technology, Allahabad, India. His research interests include control systems,

electronic circuits, networked control systems, and practical applications of control system theory, antenna theory.



Ramesh Kumar Verma is born on 15, June 1985 in Ambedkar Nagar, Uttar Pradesh India. He is currently pursuing Ph.D from AKTU Lucknow, Uttar Pradesh India. He had completed M.Tech in the year 2015 from Bundelkhand Institute of Engineering and Technology Jhansi, in digital communication. He had completed B.Tech in the year 2009 from Raj Kumar Goel Institute of Technology Ghaziabad in electronics and communication engineering. He is an expert in antenna designing, fabrication, IE3D simulation software and particle swarm optimization (PSO) algorithm. Presently he is working on optimization of microstrip patch antenna with PSO and curve fitting.